Physica D 300 (2015) 41–50

Contents lists available at ScienceDirect

Physica D

journal homepage: www.elsevier.com/locate/physd

Effects of interactions on the dynamics of driven cold atoms

Alexandra Bakman *, Shmuel Fishman

Physics Department, Technion- Israel Institute of Technology, Haifa 3200, Israel

HIGHLIGHTS

- The effects of interactions on quantum fidelity were studied for kicked particles.
- Three fidelity periods were found.
- The shortest and longest periods appear both with and without interactions.
- The intermediate period appears only in the presence of interactions.
- All these oscillations are of classical origin.

ARTICLE INFO

Article history:
Received 21 August 2014
Received in revised form
9 February 2015
Accepted 23 February 2015
Available online 2 March 2015
Communicated by V.M. Perez-Garcia

Keywords:
Fidelity
BEC
Cold atoms
Classical
GPE

ABSTRACT

The quantum fidelity was introduced by Peres to study some fingerprints of classically chaotic behavior in the quantum dynamics of the corresponding systems. In the present paper the signatures of classical dynamics near elliptic points and of interactions between particles are characterized for kicked systems. In particular, the period of the fidelity resulting of the interactions is found using analytical and numerical calculations. A mechanism leading to the oscillations with the intermediate period is proposed. It is of a classical origin and results of the interplay between the oscillations of the width of the wave packets and the rotation of their center around the elliptic fixed point.

1. Introduction

Effects of inter-particle interactions on the dynamics of driven systems were the subject of several recent works [1–4]. In the present paper these studies will be extended to the exploration of the effects of interactions on the quantum fidelity.

The concept of quantum fidelity was introduced by Peres [5] as a fingerprint of classical chaos in quantum dynamics. It has subsequently been extensively utilized in theoretical [6–9] and experimental studies [9–12] (for a review see [13]). In absence of interactions the quantum fidelity, in a mixed system (in some parts of phase space the dynamics is chaotic and in other parts it is regular), was studied [14]. In particular, it was found that the fidelity exhibits oscillations in time, and their periods are found to be related to the periods of the motion in regular parts of phase space [14].

In the present work we will study the effects of the inter-particle interactions on the periods of the fidelity. The fidelity is defined by

$$F(t) = |\langle\psi_1|\psi_2\rangle|^2 \tag{1}$$

where

$$|\psi_1(t)\rangle = e^{i\frac{H_1 t}{\hbar}}|\phi_0\rangle \tag{2}$$

and

$$|\psi_2(t)\rangle = e^{i\frac{H_2 t}{\hbar}}|\phi_0\rangle \tag{3}$$

are propagated by the Hamiltonians H_1 and H_2, that are of the same form but with different values of the parameters and $|\phi_0\rangle$ is the initial state.

We note that the fidelity $F(t)$ is related to the integral over Wigner functions,

$$F(t) = \int_{-\infty}^{\infty}\int_{-\infty}^{\infty} dxdpW_1(x,p)\,W_2(x,p) \tag{4}$$

where W_1 and W_2 are the Wigner functions of $|\psi_1\rangle$ and $|\psi_2\rangle$, respectively.

* Corresponding author.
E-mail address: sashabak@tx.technion.ac.il (A. Bakman).

http://dx.doi.org/10.1016/j.physd.2015.02.006
0167-2789/

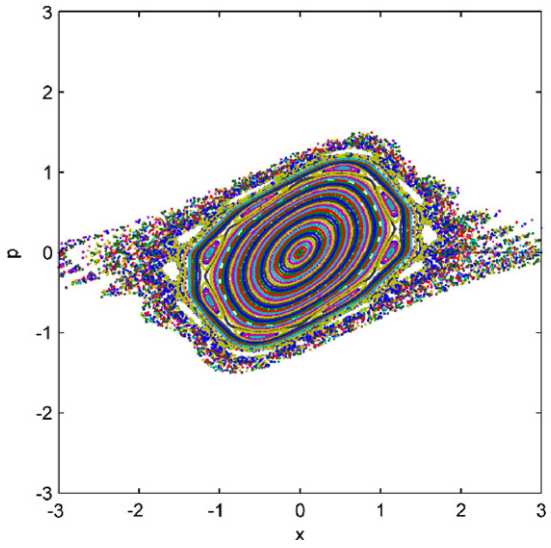

Fig. 1. The phase portrait for $K = 1$. Colors distinguish different orbits. (For interpretation of the references to color in this figure legend, the reader is referred to the web version of this article.)

The general form of the Wigner function is

$$W(x,p) = \frac{1}{\pi \cdot \hbar} \int_{-\infty}^{\infty} d\xi \cdot \psi^*(x+\xi)\, \psi(x-\xi)\, e^{\frac{2ip\xi}{\hbar}}. \tag{5}$$

Without interactions, the specific system we will study is defined by the Hamiltonian [14]

$$H = \frac{p^2}{2} - Ke^{-\frac{x^2}{2}} \sum_{n=-\infty}^{\infty} \delta(t-n) \tag{6}$$

where

$$p = -i\tau\partial_x \tag{7}$$

and

$$\tau = \frac{\hbar T}{m\Delta^2} \tag{8}$$

is the rescaled $\hbar$, satisfying

$$[x,p] = i\tau. \tag{9}$$

The Hamiltonian is in dimensionless units. The strength of the kicking potential is K, also called the stochasticity parameter, a term that will be used in the present paper. In physical units T is the time between the kicks, $\triangle$ is the width of the pulses of the kicking potential, while m is the mass of the particles. The scaling transformation between the physical and dimensionless units used here is $\frac{x}{\Delta} \to x$, $\frac{t}{T} \to t$, $\frac{pT}{m\Delta} \to p$, $\frac{KT^2}{m\Delta^2} \to K$. The one step evolution operator is

$$U = e^{-i\frac{p^2}{2\tau}} \exp\left(i\frac{K}{\tau}e^{-\frac{x^2}{2}}\right). \tag{10}$$

The corresponding classical map is

$$p_{n+1} = p_n - Kx_n e^{-\frac{x_n^2}{2}} \tag{11}$$

$$x_{n+1} = x_n + p_{n+1}. \tag{12}$$

Its phase portrait is shown in Fig. 1.

In previous explorations [15] the interaction term was introduced only between the kicks and the $\frac{p^2}{2}$ term was replaced by

$$H_I = \frac{p^2}{2} + \beta|\psi(x)|^2 \tag{13}$$

where β is the strength of the interactions. Therefore, between the kicks the dynamics are modeled by the nonlinear Schrödinger equation (NLSE), known also as the Gross Pitaevskii equation (GPE),

$$i\tau\frac{\partial\psi}{\partial t} = H_I\psi. \tag{14}$$

In the expression for the evolution operator U of (10), $e^{-\frac{p^2}{2\tau}}$ should be replaced by another evolution operator. In the calculation of the fidelity [15], the frequencies that were found in the absence of interactions were observed. In addition, a different new frequency was found. Unlike the other frequencies, this frequency is not related in any simple way to the frequencies of the underlying classical system. It was found to depend on the strength of the inter-particle interactions and can be considered as a signature of the interactions in the fidelity.

The main problem with introducing the interaction term between kicks [15] is that it requires the numerical solution of the NLSE in each interval between kicks. This process is highly time consuming since it requires the solution of a differential equation between the kicks, and it is impossible to propagate the system for very long times.

For this reason, in the current work we study a model that is defined by the evolution operator

$$U = e^{-i\frac{p^2}{2\tau}} \exp\left(\frac{i}{\tau}\left(Ke^{-\frac{x^2}{2}} + \beta|\psi(x)|^2\right)\right) \tag{15}$$

where the interactions are introduced at the kicks. The Hamiltonian of this model is

$$H = \frac{p^2}{2} - Ke^{-\frac{x^2}{2}} \sum_{n=-\infty}^{\infty} \delta(t-n) + \beta|\psi(x)|^2 \sum_{n=-\infty}^{\infty} \delta(t-n). \tag{16}$$

This model is related to one studied by Shepelyansky [16].

To the best of our knowledge, this model is difficult to realize in present experiments. Consequently, the purpose of this study is purely theoretical, with the aim to shed light on the fingerprints of interparticle interactions in the fidelity. We will focus our studies on the fidelity oscillations for wavepackets started near the central elliptic fixed point. It will turn out that periods of some of the oscillations are very long. Therefore, in order to extract them from the wavepacket evolution, it has to be followed for times that are much longer than the periods. This approach is impractical if one has to follow the evolution of (13) between the kicks. On the other hand it can be more easily done for the model defined in (15) and studied in the present work.

In Section 2 we will introduce a harmonic oscillator model describing the motion near the fixed point and discuss the modifications required. In Section 3 we will introduce an approximate theory for the fidelity oscillations and in Sections 4 and 5 we will confront it with numerical results. The results are summarized and discussed in Section 6.

2. A model for the motion near the central elliptic point

Near the fixed point $(x,p) = (0,0)$, the dynamics are approximately determined by the tangent map of the fixed point. For this purpose we linearize the classical map (11)–(12) around the fixed point $x = p = 0$. This gives the equation for the deviations from this point

$$\begin{pmatrix}\delta x_{n+1}\\ \delta p_{n+1}\end{pmatrix} = \begin{pmatrix}(1-K) & 1\\ -K & 1\end{pmatrix}\begin{pmatrix}\delta x_n\\ \delta p_n\end{pmatrix}. \tag{17}$$

The eigenvalues of this map are

$$\alpha_\pm = \frac{(2-K)}{2} \pm \frac{\sqrt{K(4-K)}}{2} \equiv e^{\pm i\omega} \tag{18}$$

with

$$\omega = \arctan\left(\frac{\sqrt{K(4-K)}}{2-K}\right), \tag{19}$$

which is the angular velocity of the points around the origin. In the vicinity of the fixed point, the system behaves like a harmonic oscillator with a frequency ω. Classically, the motion of the trajectories, starting near the elliptic fixed point, $x = p = 0$, stays there because the region is bounded by curves that surround this point. The existence of such curves is a corollary of the KAM (Kolmogorov-Arnold-Moser) theorem. We consider here two Hamiltonians H_1 and H_2 that differ only by the values of the stochasticity parameter K, taking the values $K_1 = 1$ and $K_2 = 1.01$. For $K = K_1 = 1$, one finds

$$\omega_1 = 1.047 \tag{20}$$

and for $K = K_2 = 1.01$,

$$\omega_2 = 1.053. \tag{21}$$

The parameters were chosen so that the map has a pronounced central island as shown in Fig. 1. The qualitative behavior should be similar for all $0 < K < 4$ (see [14]) and $K = 1$ is a representative value at this interval. For $\beta = 0$ and $K = 0$ the system is integrable and momentum is conserved while for $\beta = 0$ and $K > 4$ the elliptic point at the origin is replaced by a hyperbolic one.

The periods of the regular trajectories deviate from the ones found at the elliptic point by (19). The deviation increases with the deviation from the elliptic point. This is similar to the situation when a small anharmonicity is added to the harmonic potential. Therefore, for wave packets initiated not exactly at the elliptic point, one has to add an anharmonic term to model the dynamics. The result is that the different parts of the packet are exposed to different frequencies. Therefore, an initially prepared Gaussian wave packet spreads in phase space. This was indeed verified for Gaussian wave packets in a harmonic well with a small anharmonic correction [17]. As the wave packet propagates, revivals are found for a very long time. Fortunately, in presence of interactions, localization of Gaussian wave packets is possible, as was found for an anharmonic well with inter-particle interactions modeled by the Gross Pitaevskii equation (GPE) [4] (see also [3]). Interactions and nonlinearity may balance each other to preserve the Gaussian wave packet [4].

In the following section, the dynamics of particles in a harmonic well with a small anharmonic perturbation will be studied analytically, for weak inter-particle interactions. Following the discussion in the present section, it will be assumed that in the vicinity of this elliptic point the motion can be described by a Gaussian wave packet.

3. Fidelity for weak interactions

In this section an estimate for the oscillations of the fidelity for a wavepacket that is initially a coherent state of a harmonic oscillator defined by the Hamiltonian

$$H = \frac{p^2}{2m} + \frac{1}{2}m\omega^2 x^2 \tag{22}$$

is discussed.

3.1. The Wigner function of a coherent state

A coherent state for the harmonic oscillator defined by the Hamiltonian (22) is [18]

$$\psi_0(x) = \left(\frac{m\omega}{\pi\hbar}\right)^{\frac{1}{4}} \exp\left(\frac{i}{\hbar}p_0(t) - \frac{m\omega}{2\hbar}(x - x_0(t))^2\right) \times e^{-\frac{i}{2\hbar}x_0\cdot p_0} e^{-i\frac{\omega t}{2}} \tag{23}$$

where $x_0(t)$ and $p_0(t)$ denote the classical trajectory in phase space. The state (23) is an eigenstate of the annihilation operator and satisfies the time dependent Schrödinger equation

$$i\hbar\frac{\partial\psi_0}{\partial t} = -\frac{\hbar^2}{2m}\frac{\partial^2\psi_0}{\partial x^2} + \frac{1}{2}m\omega^2 x^2\psi_0. \tag{24}$$

The Wigner function of this coherent state is found from the definition (5):

$$W_0(x, p) = \frac{1}{\pi\cdot\hbar} e^{-\frac{m\omega}{\hbar}(x-x_0)^2} e^{-\frac{(p-p_0)^2}{m\omega\hbar}}. \tag{25}$$

3.2. The fidelity for coherent states in absence of interactions

Let ω_1 and ω_2 be the frequencies of two harmonic oscillators, whose potentials differ slightly. The Wigner functions for these wavefunctions are ($i = 1, 2$)

$$W_i(x, p) = \frac{1}{2\pi\sigma_{x_i}\sigma_{p_i}} \times \exp\left(-\frac{1}{2}\left(\frac{(x - x_i(t))^2}{\sigma_{x_i}^2} + \frac{(p - p_i(t))^2}{\sigma_{p_i}^2}\right)\right) \tag{26}$$

where

$$\sigma_{x_i}^2 = \frac{\hbar}{2m\omega_i} \tag{27}$$

and

$$\sigma_{p_i}^2 = \frac{m\omega_i\hbar}{2}. \tag{28}$$

The fidelity in absence of interactions is calculated using (4) and is given by

$$F = Ce^{-\frac{1}{2}(s_x + s_p)} \tag{29}$$

where the parameters are given by

$$C = \frac{2}{\pi\hbar^2}\sqrt{\frac{\sigma_{x_1}^2\sigma_{x_2}^2\sigma_{p_1}^2\sigma_{p_2}^2}{\left(\sigma_{x_1}^2 + \sigma_{x_2}^2\right)\left(\sigma_{p_1}^2 + \sigma_{p_2}^2\right)}} \tag{30}$$

$$s_x = \frac{(x_1(t) - x_2(t))^2}{\sigma_{x_1}^2 + \sigma_{x_2}^2} \tag{31}$$

$$s_p = \frac{(p_1(t) - p_2(t))^2}{\sigma_{p_1}^2 + \sigma_{p_2}^2}. \tag{32}$$

The classical trajectories are given by

$$(x_1, p_1) = \rho\left[\cos(\omega_1 t), -m\omega_1\sin(\omega_1 t)\right] \tag{33}$$

and

$$(x_2, p_2) = \rho\left[\cos(\omega_2 t), -m\omega_2\sin(\omega_2 t)\right] \tag{34}$$

where

$$\rho = x_1(0) = x_2(0). \tag{35}$$

Therefore, (31) can be written in the form

$$s_x = \frac{\rho^2}{\sigma_{x_1}^2 + \sigma_{x_2}^2}\left(1 + \frac{1}{2}(\cos(2\omega_1 t) + \cos(2\omega_2 t)) - \cos(\delta\omega\cdot t) - \cos(\omega_s t)\right) \tag{36}$$

where

$$\omega_s = \omega_1 + \omega_2 \tag{37}$$

and

$$\delta\omega = \omega_2 - \omega_1. \tag{38}$$

Similarly,

$$s_p = \frac{\rho^2 m^2}{\sigma_{p_1}^2 + \sigma_{p_2}^2} \times \left(\frac{\omega_1^2 + \omega_2^2}{2} - \frac{1}{2}\left(\omega_1^2 \cos(2\omega_1 t) + \omega_2^2 \cos(2\omega_2 t)\right)\right) + \frac{\rho^2 m^2}{\sigma_{p_1}^2 + \sigma_{p_2}^2}\left(\omega_1\omega_2 \cos(\delta\omega \cdot t) - \omega_1\omega_2 \cos(\omega_s t)\right). \quad (39)$$

For the model (6) we study here, for $K_1 = 1$ and $K_2 = 1.01$, we find from (20) and (21) that

$$\delta\omega = 0.0057747. \quad (40)$$

3.3. The fidelity for coherent states with weak interactions

We assume that the main effect of interactions is on the width of the wave packets.
The width of the wave packet is defined as

$$\langle \Delta x \rangle^2 = \left\langle (x - \langle x \rangle)^2 \right\rangle, \quad (41)$$

where $\langle O \rangle = \int_{-\infty}^{\infty} dx \psi^* O \psi$.

Since we assume that the interactions are weak, the resulting correction is expected to be small. We assume that the variation is periodic, with a period Ω_i close to $2\omega_i$, an assumption that will be verified numerically. A motivation for such an assumption is that the expression for the width (41) involves only the combinations of frequencies $\omega_1 \pm \omega_2$, $2\omega_1$ and $2\omega_2$. Following this assumption, we replace (27) and (28) by

$$\tilde{\sigma}_{x_1}^2 = \sigma_x^2 + \gamma_x \cos(\Omega_1 t + \phi_x) \quad (42)$$

$$\tilde{\sigma}_{x_2}^2 = \sigma_x^2 + \gamma_x \cos(\Omega_2 t + \phi_x) \quad (43)$$

and

$$\tilde{\sigma}_{p_1}^2 = \sigma_p^2 + \gamma_p \cos\left(\Omega_1 t + \phi_p\right) \quad (44)$$

$$\tilde{\sigma}_{p_2}^2 = \sigma_p^2 + \gamma_p \cos\left(\Omega_2 t + \phi_p\right), \quad (45)$$

resulting in

$$s_x = \frac{\rho^2}{2\sigma_x^2}\left(\cos(\omega_1 t) - \cos(\omega_2 t)\right)^2 \times \left(1 + \frac{\gamma_x}{2\sigma_x^2}\left(\cos(\Omega_1 t + \phi_x) + \cos(\Omega_2 + \phi_x)\right)\right)^{-1}. \quad (46)$$

Similarly for s_p,

$$s_p = \frac{\rho^2 m^2}{2\sigma_p^2}\left(\omega_1 \sin(\omega_1 t) + \omega_2 \sin(\omega_2 t)\right)^2 \times \left(1 + \frac{\gamma_p}{2\sigma_p^2}\left(\cos\left(\Omega_1 t + \phi_p\right) + \cos\left(\Omega_2 t + \phi_p\right)\right)\right)^{-1}. \quad (47)$$

We assume that the corrections resulting of the interactions are small, therefore even with the replacement $\sigma \to \tilde{\sigma}$ the states ψ_i are within a good approximation similar to coherent states. We assume also

$$\sigma_{x_1} \approx \sigma_{x_2} \approx \sigma_x \quad (48)$$

and

$$\sigma_{p_1} \approx \sigma_{p_2} \approx \sigma_p. \quad (49)$$

This assumption is consistent with (51) and this is the condition when fidelity is studied. γ_x and γ_p are the width oscillation amplitudes in position and momentum respectively. Since $\beta \ll 1$, we assume $\left|\frac{\gamma_x}{2\sigma_x^2}\right| \ll 1$ and $\left|\frac{\gamma_p}{2\sigma_p^2}\right| \ll 1$. In the leading order in $\frac{\gamma_x}{2\sigma_x^2}$ and $\frac{\gamma_p}{2\sigma_p^2}$ one can simplify the expression as it is done in Appendix A.

Our crucial assumption is that the Wigner function is well approximated by a Gaussian wave packet. In the presence of interactions it is possible that such a wave packet is stable in spite of the effective anharmonicity generated for kicked systems, defined by (6) as well as by (15)–(16) (see [4]). In our case, where the interactions are weak, the frequency of the width oscillation satisfies

$$\Omega_1 \approx \Omega_2 \equiv \Omega, \quad (50)$$

$$\omega_1 \approx \omega_2 \equiv \omega \quad (51)$$

and

$$\Omega_{1,2} \approx \omega_{1,2} \gg \delta\omega. \quad (52)$$

We denote

$$\omega_s = \omega_1 + \omega_2 \approx 2\omega. \quad (53)$$

Using the approximation in (53), we denote

$$\Delta\omega = \omega_s - \Omega \approx 2\omega - \Omega. \quad (54)$$

we find (see Appendix A)

$$s_x + s_p = \sum_{i=1}^{8} A_i \quad (55)$$

where

$$A_1 = \frac{\rho^2}{2\sigma_x^2} + \frac{\rho^2 m^2 \omega^2}{2\sigma_p^2}, \quad (56)$$

$$A_2 = \left(-\frac{\rho^2}{2\sigma_x^2} + \frac{\rho^2 m^2 \omega^2}{2\sigma_p^2}\right)\cos(\delta\omega \cdot t), \quad (57)$$

$$A_3 = -\frac{\rho^2 m^2 \omega^2}{\sigma_p^2}\cos(\omega_s \cdot t), \quad (58)$$

$$A_4 = \frac{\rho^2 \gamma_x}{2\sigma_x^4}\cos(\Omega \cdot t + \phi_x) - \frac{\rho^2 \gamma_p m^2 \omega^2}{2\sigma_p^4}\cos\left(\Omega \cdot t + \phi_p\right), \quad (59)$$

$$A_5 = \frac{\rho^2 \gamma_x}{4\sigma_x^4}\cos\left((\Omega + \delta\omega)t + \phi_x\right) - \frac{\rho^2 m^2 \gamma_p \omega^2}{4\sigma_p^4}\cos\left((\Omega + \delta\omega)t + \phi_p\right), \quad (60)$$

$$A_6 = \frac{\rho^2 \gamma_x}{4\sigma_x^4}\cos\left((\Omega - \delta\omega)t + \phi_x\right) - \frac{\rho^2 m^2 \gamma_p \omega^2}{4\sigma_p^4}\cos\left((\Omega - \delta\omega)t + \phi_p\right), \quad (61)$$

$$A_7 = \frac{\rho^2 m^2 \gamma_p \omega^2}{2\sigma_p^4}\cos\left(\Delta\omega t - \phi_p\right) \quad (62)$$

and

$$A_8 = \frac{\rho^2 m^2 \gamma_p \omega^2}{2\sigma_p^4}\cos\left((\omega_s + \Omega)t + \phi_p\right). \quad (63)$$

The difference $\delta\omega$ sets the long period of the fidelity, and results from the difference between the two Hamiltonians. The frequency $2\omega \approx \omega_s$ is twice the frequency of rotation around the fixed point at the origin. The overall coefficient corresponding to the intermediate angular velocity $\Delta\omega$ is $\frac{\rho^2 m^2 \gamma_p \omega^2}{2\sigma_p^4}$.

The relations (53)–(54) imply that (55) with (55)–(63) oscillate with three different frequencies: ω_s, $\Delta\omega$ and $\delta\omega$, which are very different, and satisfy $\omega_s \gg \Delta\omega \gg \delta\omega$. The corresponding periods will be denoted by

$$T_1 = \frac{2\pi}{\omega_s} \quad (64)$$

$$T_2 = \frac{2\pi}{\Delta\omega} \quad (65)$$

and

$$T_3 = \frac{2\pi}{\delta\omega}. \tag{66}$$

The frequencies ω_s and $\delta\omega$ (and consequently T_1 and T_3), depend only on the classical frequencies ω_1 and ω_2. The frequency $\Delta\omega$ depends on Ω that is not related to any of the other classical frequencies.

Note that also harmonics of these three basic frequencies may be present. Since this is a very heuristic theory, also deviations and splitting of the frequency peaks are expected.

4. Fidelity oscillations

In this section we present oscillations of the fidelity. In previous work [14], the fidelity oscillations in absence of interactions were calculated. In particular, there were identified two frequencies. These frequencies are of pure classical origin. One of them, denoted by ω_s, is related to the classical motion around the elliptic fixed point. The second frequency is $\delta\omega$. These frequencies were found for $\beta = 0$ and reported in [14]. In presence of interactions an intermediate frequency ω_I absent in [14] is found. In this section we report the numerical values of these frequencies for various values of parameters.

In all calculations presented here we used two Hamiltonians of the form (16) with the values of the stochasticity parameter K that takes values that are close, namely, $K_1 = 1$ and $K_2 = 1.01$. We launched an initial wave packet of the form (23) for various initial values $x_0\,(t=0)$ and $p_0\,(t=0)$. Each wave packet was iterated using the one step propagator (15). The fidelity was calculated from (1). Plots of the form of Fig. 2(a) with the corresponding Fourier transform in Fig. 2(b)

$$\hat{F}\,(\nu) = \int_{-\infty}^{\infty} F\,(t)\, e^{-i2\pi\nu t} dt \tag{67}$$

were generated. The dominant frequencies are marked by arrows in Fig. 2(b). We repeated the calculation for different initial values of $x_0\,(t=0)$, $p_0\,(t=0)$ and β.

From Fig. 2 we found numerically that the fidelity exhibits three frequencies: a large frequency $\nu_1 \approx 0.33\left[kicks^{-1}\right]$, corresponding to period $T_1 \approx 3\,[kicks]$; an intermediate frequency, $\nu_2 \approx 0.025\left[kicks^{-1}\right]$, corresponding to $T_2 \approx 40\,[kicks]$; and a small frequency $\nu_3 \approx 0.001\left[kicks^{-1}\right]$, corresponding to $T_3 \approx 1000\,[kicks]$. These results were repeated for various initial values of $x_0\,(t=0)$, $p_0\,(t=0)$ and β and are presented in Figs. 3–4. In Fig. 3, the periods T_1, T_2 and T_3 found from plots similar to the ones presented in Fig. 2, are plotted as a function of β for $(x_0\,(t=0)\,,\,p_0\,(t=0)) = (0.18, 0)$ and $\tau = 0.01$. Similar results are found for various initial conditions such that $x_0\,(t=0) \geq 0.14$, $p_0\,(t=0) = 0$ and $\tau = 0.01$. Note that T_1 is slowly increasing with β.

From Fig. 4, the periods T_1, T_2 and T_3 as function of $x_0\,(t=0)$ are presented for $p_0\,(t=0) = 0$, $\beta = 6\cdot 10^{-5}$ and $\tau = 0.01$. The results for $x_0\,(t=0) = 0$, $p_0\,(t=0) \neq 0$ are similar.

In all situations we found that the period T_1 varies between 3 and 3.05 kicks. It is very close to the value $T_1 = \frac{2\pi}{\omega_s} \simeq \frac{\pi}{\omega_1} = 3$ kicks, where ω_1 is given by (20). The period is systematically increasing with $x_0\,(t=0)$ and $p_0\,(t=0)$ (see Fig. 4(a)). The reason is the deviation of the frequency from the value found in the vicinity of the fixed point at the origin. This can be verified by direct iteration of the map (11)–(12).

For $x_0\,(t=0)$ that is sufficiently large, the period T_3 was found to take the value $T_3 \approx 1100$ kicks. It is close to value predicted from pure classical dynamics without interactions, $T_3 = 1091.8$ kicks for $K_1 = 1$ and $K_2 = 1.01$, calculated using (66). For $x_0\,(t=0) = p_0\,(t=0) = 0$, we expect that $T_3 = \frac{\pi}{\delta\omega}$, rather than $\frac{2\pi}{\delta\omega}$. This is because of the symmetry of the initial condition. Each point of a trajectory generated by H_1 is chasing a point generated by H_2 which is its reflection through the origin of the phase space and, therefore, is found first at an angle of π and not 2π. Indeed, this was found for sufficiently small $x_0\,(t=0)$ (see Fig. 4(c)).

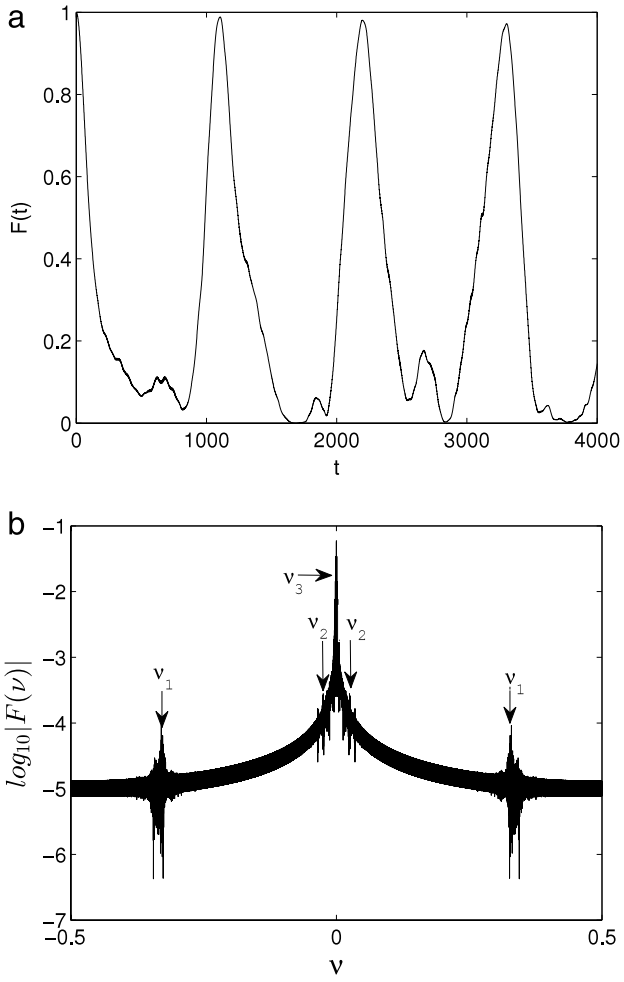

Fig. 2. The fidelity for $(x_0\,(t=0)\,,\,p_0\,(t=0)) = (0.18, 0)$, $\beta = 6\cdot 10^{-5}$ and $\tau = 0.01$ (a) as function of number of kicks; (b) $\log_{10}|\hat{F}\,(\nu)|$ as a function of the inverse number of kicks ν.

In summary, the periods T_1 and T_3 are of pure classical origin. These were found in [14] in absence of interactions. Here we found that these are weakly affected by the interactions. The intermediate period T_2 is found to be $T_2 \approx 40$ kicks (see Figs. 3(b), and 4(b)). This period was not found in absence of interactions.

We turn now to the exploration of the origin of the intermediate period T_2.

5. The origins of the intermediate period

In this section we will demonstrate that the intermediate period results from the oscillation of the width of the wavefunction. The Fourier transform of the width (41)

$$\hat{f}_{\Delta}\,(\omega) = \int_{-\infty}^{\infty} \langle \Delta x\,(t)\rangle^2\, e^{-i2\omega t} dt \tag{68}$$

was computed for ψ which was derived from an initially coherent state of the form (23) by application of the evolution operator (15). We found that it exhibits the peaks $T_1 = 3.05\,[kicks]$ $\left(\omega_1 \simeq \omega = 2.06\left[\frac{1}{kick}\right]\right)$, $T_{width} = 3.24\,[kicks]$ and $\Omega_{width} = 1.94\left[\frac{1}{kick}\right]$ for $\beta = 6\cdot 10^{-5}$, $\tau = 0.01$, $(x_0\,(t=0)\,,\,p_0\,(t=0)) = (0, 0.14)$ and for $(x_0\,(t=0)\,,\,p_0\,(t=0)) = (0.18, 0)$.

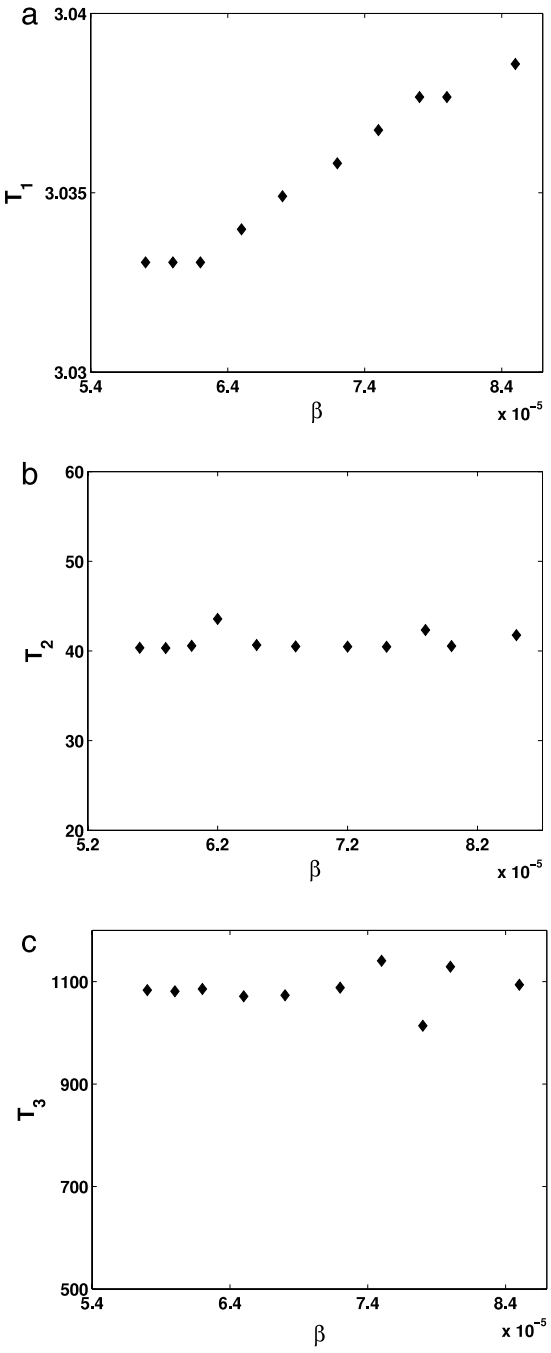

Fig. 3. Various periods of the fidelity as a function of β for $(x_0\ (t=0)\ ,\ p_0\ (t=0))$ $= (0.18, 0)$ and $\tau = 0.01$. (a) T_1; (b) T_2; (c) T_3.

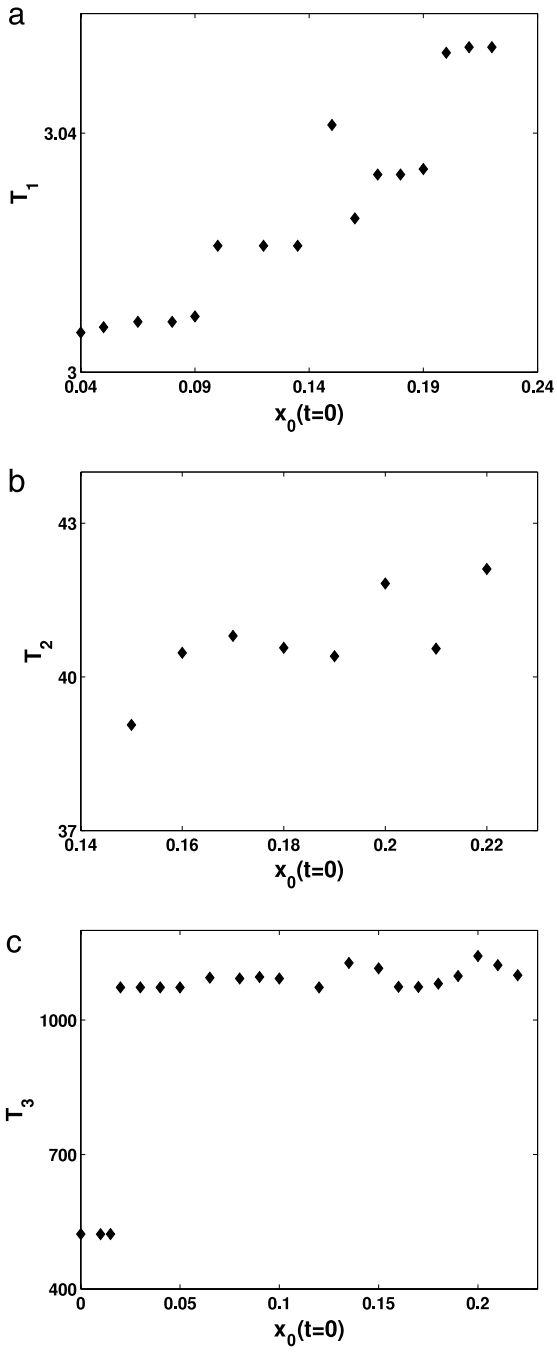

Fig. 4. Various periods of the fidelity as a function of $x_0\ (t=0)$ for $p_0\ (t=0) = 0$, $\beta = 6 \cdot 10^{-5}$ and $\tau = 0.01$. (a) T_1; (b) T_2; (c) T_3.

We note that indeed Ω_{width} which was found numerically is close to 2ω. Taking $\Omega = \Omega_{width}$, we use (54) to calculate

$$\Delta\omega = 2\omega - \Omega_{width}, \tag{69}$$

and find the predicted intermediate period $T_2^{(p)} = \frac{2\pi}{\Delta\omega}$, where Ω_{width} is found from the numerical calculations of (68). Comparison between this value and T_2 calculated from the fidelity Fourier transform (67) is shown in Fig. 5. The difference is small, as expected from Section 3.3. The period T_2 is practically independent of β. In the limit $\beta \to 0$ the amplitude of the fidelity component corresponding to this period vanishes.

The generation of the intermediate period is not characteristic of the fidelity but will show up in any correlation function involving overlap of Wigner functions. The fidelity is the overlap of Wigner functions at the same time but different Hamiltonians. Similar behavior is found for overlap of the Wigner functions for the same Hamiltonian but at different times n and $n - \Delta n$ defined by

$$G\,(n) = \iint_{-\infty}^{\infty} W_n\,(x,\,p)\,W_{n-\Delta n}\,(x,\,p)\,dxdp \tag{70}$$

and is calculated in detail in Appendix B.

First, we note that the Wigner function rotates around the elliptic point as demonstrated in Fig. 6 for 990–995 kicks. In Fig. 6(a) we see that for $\beta = 0$ the function shape is more spread

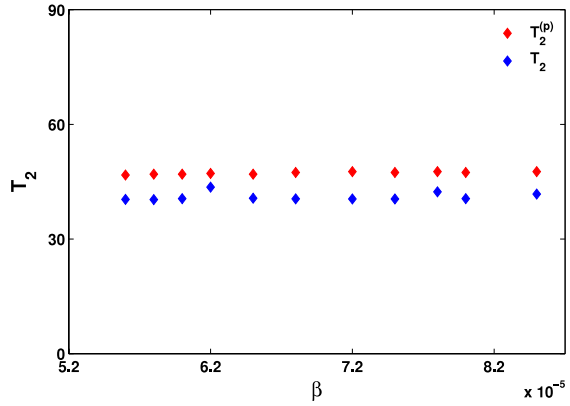

Fig. 5. The predicted intermediate period of the fidelity $T_2^{(p)}$ compared to T_2, found directly from the Fourier transform of the fidelity, as function of β, for $(x_0\,(t=0)\,, p_0\,(t=0)) = (0.18, 0)$ and $\tau = 0.01$. (For interpretation of the references to color in this figure legend, the reader is referred to the web version of this article.)

over the phase space than in Fig. 6(b). In this case interactions tend to localize the Wigner function in phase space, similar to the results of [4]. The Wigner function oscillates with various periods. The most prominent is

$$T_{W_1} = \frac{2\pi}{\omega}, \tag{71}$$

(see (51) and (53)). Therefore,

$$T_{W_1} = \frac{2\pi}{\frac{\omega_s}{2}} = 2T_1. \tag{72}$$

In our case, $T_1 \approx 3\,[kicks]$ kicks, as can be seen from Figs. 3(a) and 4(a). From (72) we see that $T_{W_1} \approx 6\,[kicks]$. Therefore, in Fig. 6 we present the rotation of the Wigner function in phase space for 6 consecutive steps. To a good approximation it is periodic with the period of 6 kicks. In Fig. 6(a) and (b) Wigner functions are presented in absence ($\beta = 0$) and presence ($\beta \neq 0$) of interactions, respectively. For $\beta \neq 0$ the Wigner function exhibits width oscillations with the period $\frac{2\pi}{\Omega_{width}}$, as expected from (46) and (47). In order to extract Ω_{width} from the dynamics of the Wigner function we calculate the Fourier transform of (70). In order to eliminate the effect of the short period $T_{W_1} \approx 6\,[kicks]$, we take $\Delta n = 6$ in (70). For $\beta = 6 \cdot 10^{-5}$ we found that $\Omega_{width} = 1.92\left[\frac{1}{kick}\right]$. From (68) we find a similar value $\Omega_{width} = 1.94\left[\frac{1}{kick}\right]$ for the same value of β. Oscillations of this frequency are absent for $\beta = 0$. This result combined with (69) and Fig. 5 provides evidence that the intermediate period T_2 is generated by the width oscillations and these result from the interactions.

It looks like the width oscillations, at least in the leading order discussed here, are of classical origin since the term $\beta\,|\psi|^2$ in (15)–(16) acts as an effective potential. Moreover, the width is a coarse grained property of the Wigner function and therefore does not depend on fine details. Hence, it approaches the value found for the corresponding classical phase space distribution.

6. Summary and discussion

The effects of weak inter-particle interactions on the quantum fidelity were calculated for kicked particles. The calculation was performed for a specific model where the interaction was introduced during the kicks. The results were found to be qualitatively similar to the ones found where the interactions were introduced between kicks [15]. We found that the fidelity periods that were obtained in absence of the interactions, namely, T_1 and T_3, are found also in the presence of the interactions. In presence of the interactions, another period, namely, T_2, was found. We explored the mechanism of the generation of this frequency. It results of the interplay of the oscillations of the width of the wave function (or Wigner function) in phase space and the rotation of its center around the elliptic fixed point. It is $\Delta\omega$ of (54) that was derived in the framework of the heuristic model outlined in Section 3 and tested numerically in Section 5. In Fig. 6 it was verified that the heuristic picture of Section 3 holds for the model of the kicked particles (15)–(16) presented in the introduction. The frequencies $\omega_1 \approx \omega_2$, ω_s and Ω_{width} found in this work for the fidelity are found also for other correlations of Wigner functions.

In this work we focused on dynamics of wave packets in the vicinity of the elliptic fixed point $(x, p) = (0, 0)$ for the classical phase portrait shown in Fig. 1.

The existence of the intermediate frequency $\Delta\omega$ ((54)) and its origin is the main result of this paper. It is plausible that the origin of this frequency is classical. This conclusion is supported also by the results of [4]. The reason is that the term $\beta\,|\psi\,(x)|^2$ in (13), (15) and (16) acts as a potential. The intermediate frequency is not found numerically if the center of the wave packet is too close to the elliptic fixed point. A possible explanation is that in such a situation one does not have the possibility to separate the rotations of the center of the packet and the oscillation of the width, a separation assumed in the derivation of (54). As one increases the distance of the wave packet from the fixed point at the origin while keeping the nonlinearity fixed, the variation of the rotation frequency increases due to the nonlinearity and the packet spreads over a ring in phase space, as is the case for $\beta = 0$ (see Fig. 6(a)). In such a situation the picture of Section 3 is violated, and indeed the amplitude of the component related to the intermediate period T_2 vanishes in the limit $\beta \to 0$.

In typical realistic models the nonlinearity in the wave function modeling the interparticle interactions should be present both at the kicks and between them. For short times it was possible to evolve wave packets for a model where the nonlinear term was present only between the kicks [15] and the obtained results were qualitatively similar to the ones we found. For the model discussed in [15] it was not feasible to compute the wave packet evolution for times much longer than T_2. Therefore, in the present work the calculations were performed for the model (15)–(16). We believe that similar results hold for a model where a nonlinear term is found both at the kicks and between them as well as for different models for the interactions present at the kicks. Exploration of this more general problem will be subject of further studies that will require substantial improvement of the numerical methods.

Acknowledgments

It is our great pleasure to thank Dr. Mark Herrera for illuminating, inspiring and critical discussions and communications. This work was partly supported by the Israel Science Foundation (ISF), Grant number 1028/12, by the US–Israel Binational Science Foundation (BSF), Grant number 2010132, by the Minerva Center of Nonlinear Physics of Complex Systems, by the New York Metropolitan Fund and by the Shlomo Kaplansky academic chair.

Appendix A. Fidelity calculation details

Eqs. (46) and (47) are simplified by means of a Taylor expansion

$$\frac{1}{1-x} \simeq 1 + x + O\left(x^2\right), \tag{A.1}$$

combined with

$$\cos\alpha \cdot \cos\beta = \frac{1}{2}\left(\cos\left(\alpha - \beta\right) + \cos\left(\alpha + \beta\right)\right), \tag{A.2}$$

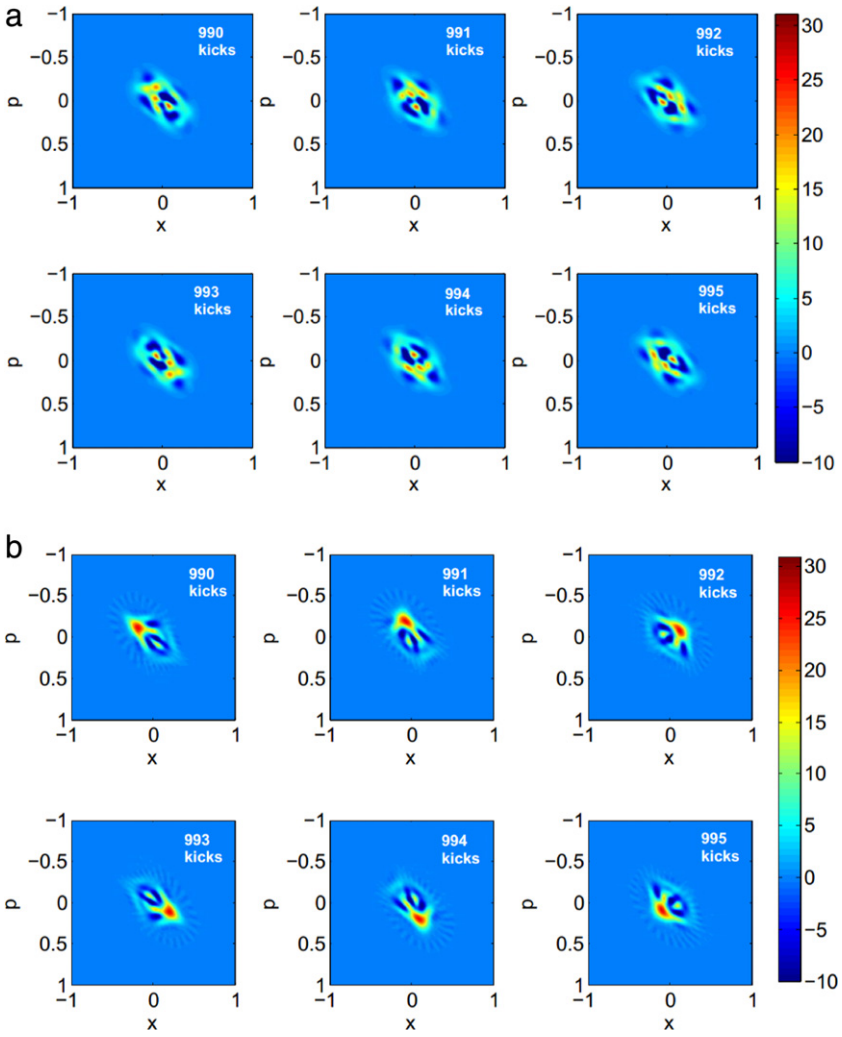

Fig. 6. The Wigner function for 990–995 kicks for $(x_0, p_0) = (0.18, 0)$, $\beta = 6 \cdot 10^{-5}$ and $\tau = 0.01$. (a) $\beta = 0$; (b) $\beta = 6 \cdot 10^{-5}$. (For interpretation of the references to color in this figure legend, the reader is referred to the web version of this article.)

the equations take the form

$$s_x = \frac{\rho^2}{2\sigma_x^2} - \frac{\rho^2}{2\sigma_x^2}\cos(\delta\omega \cdot t) + \frac{\rho^2\nu}{4\sigma_x^4}\cos((\Omega + \delta\omega)t + \phi_x) + \frac{\rho^2\nu}{4\sigma_x^4}\cos((\Omega - \delta\omega)t + \phi_x) - \frac{\rho^2\nu}{2\sigma_x^4}\cos(\Omega \cdot t + \phi_x) \quad \text{(A.3)}$$

and

$$\begin{aligned} s_p = {} & \frac{\rho^2 m^2\omega^2}{2\sigma_p^2} - \frac{\rho^2 m^2\omega^2}{\sigma_p^2}\cos(2\omega \cdot t) + \frac{\rho^2 m^2\omega^2}{2\sigma_p^2}\cos(\delta\omega \cdot t) \\ & + \frac{\rho^2 m^2\gamma\omega^2}{2\sigma_p^4}\cos\left((2\omega + \Omega)t + \phi_p\right) \\ & - \frac{\rho^2 m^2\gamma\omega^2}{4\sigma_p^4}\cos\left((\Omega + \delta\omega)t + \phi_p\right) \\ & - \frac{\rho^2 m^2\gamma\omega^2}{4\sigma_p^4}\cos\left((\Omega - \delta\omega)t + \phi_p\right) \\ & + \frac{\rho^2 m^2\gamma\omega^2}{2\sigma_p^4}\cos\left((2\omega + \Omega)t + \phi_p\right) \\ & - \frac{\rho^2 m^2\gamma\omega^2}{4\sigma_p^4}\cos\left((\Omega + \delta\omega)t + \phi_p\right) \\ & - \frac{\rho^2 m^2\gamma\omega^2}{4\sigma_p^4}\cos\left((\Omega - \delta\omega)t + \phi_p\right) \\ & + \frac{\rho^2 m^2\gamma\omega^2}{2\sigma_p^4}\cos\left(\Delta\omega - \phi_p\right) \\ & - \frac{\rho^2 m^2\gamma\omega^2}{2\sigma_p^4}\cos\left(\Omega \cdot t + \phi_p\right). \end{aligned} \quad \text{(A.4)}$$

From this, one finds (55)–(63).

Appendix B. Correlation of the Wigner function at various times

In this Appendix we identify the frequencies of $G(n)$ defined by (70), where Δn is fixed. The derivation is similar to the derivation of the fidelity oscillations in Section 3 and Appendix A. First, we assume that there are no interactions and then we add the effect of weak interactions. We consider wave packets near the elliptic fixed point $(x, p) = (0, 0)$ and as in the case of the fidelity we calculate $G(n)$ in continuous time for a harmonic well.

B.1. Correlation of Wigner functions for different times in absence of interactions

Let ω_1 be the frequency of a harmonic oscillator. The Wigner function of a coherent state of the oscillator (23), corresponding to a time t is (26), namely

$$W_t(x, p) = \frac{1}{2\pi\sigma_x\sigma_p} e^{-\frac{1}{2}\left(\frac{(x - x(t))^2}{\sigma_x^2} + \frac{(p - p(t))}{\sigma_p^2}\right)}. \quad \text{(B.1)}$$

The Wigner function corresponding to a time $t-\Delta t$ is

$$W_{t-\Delta t}(x,p)=\frac{1}{2\pi\sigma_x\sigma_p}e^{-\frac{1}{2}\left(\frac{(x-x(t-\Delta t))^2}{\sigma_x^2}+\frac{(p-p(t-\Delta t))^2}{\sigma_p^2}\right)}, \tag{B.2}$$

where σ_x and σ_p are given by (27) and (28) and denote the width of the Wigner function in position and momentum, respectively. The difference between the times is constant and given by Δt.
The correlation in absence of interactions is of the form

$$G=C\cdot e^{-\frac{1}{2}(s_x+s_p)} \tag{B.3}$$

with

$$C=\frac{1}{4\pi\sigma_x\sigma_p}, \tag{B.4}$$

$$s_x=\frac{(x(t)-x(t-\Delta t))^2}{2\sigma_x^2} \tag{B.5}$$

and

$$s_p=\frac{(p(t)-p(t-\Delta t))^2}{2\sigma_p^2}. \tag{B.6}$$

The phase coordinates are

$$(x(t),p(t))=\rho\left[\cos(\omega t),-m\omega\sin(\omega t)\right] \tag{B.7}$$

and

$$\begin{aligned}&(x(t-\Delta t),p(t-\Delta t))\\&\quad=\rho\left[\cos(\omega t+\phi),-m\omega\sin(\omega t+\phi)\right],\end{aligned} \tag{B.8}$$

where

$$\phi=\omega\Delta t. \tag{B.9}$$

B.2. Correlation of Wigner functions for different times with weak interactions

The width of the Wigner functions in presence of weak interactions is given by

$$\tilde{\sigma}_{x_1}^2=\sigma_x^2+\gamma_x\cos(\Omega t+\phi_x), \tag{B.10}$$

$$\tilde{\sigma}_{x_2}=\sigma_x^2+\gamma_x\cos(\Omega t+\phi_x-\Delta\phi), \tag{B.11}$$

$$\tilde{\sigma}_{p_1}=\sigma_p^2+\gamma_p\cos\left(\Omega t+\phi_p\right) \tag{B.12}$$

and

$$\tilde{\sigma}_{p_2}^2=\sigma_p^2+\gamma_p\cos\left(\Omega t+\phi_p-\Delta\phi\right), \tag{B.13}$$

where

$$\Delta\phi=\Omega\cdot\Delta t. \tag{B.14}$$

Therefore,

$$\begin{aligned}C(t)&=\left(2\pi\sigma_{x(t)}\sigma_{p(t)}\sigma_{x(t-\Delta t)}\sigma_{p(t-\Delta t)}\right)^{-1}\\&\quad\times\sqrt{\frac{\sigma_{x(t)}^2\sigma_{x(t-\Delta t)}^2\sigma_{p(t)}^2\sigma_{p(t-\Delta t)}^2}{\left(\sigma_{x(t)}^2+\sigma_{x(t-\Delta t)}^2\right)\left(\sigma_{p(t)}^2+\sigma_{p(t-\Delta t)}^2\right)}}\end{aligned} \tag{B.15}$$

and

$$G(t)=C(t)\cdot e^{-\frac{1}{2}(s_x(t)+s_p(t))}. \tag{B.16}$$

The expressions for $s_x(t)$ and $s_p(t)$ become

$$\begin{aligned}s_x(t)&=\frac{\rho^2}{2\sigma_x^2}\\&\quad\cdot\frac{(\cos(\omega t)-\cos(\omega t-\phi))^2}{1+\frac{\gamma_x}{2\sigma_x^2}\left(\cos(\Omega t+\phi_x)+\cos(\Omega t+\phi_x-\Delta\phi)\right)}\end{aligned} \tag{B.17}$$

and

$$\begin{aligned}s_p(t)&=\frac{\rho^2m^2\omega^2}{2\sigma_p^2}\\&\quad\cdot\frac{(\sin(\omega t)-\sin(\omega t-\phi))^2}{1+\frac{\gamma_p}{2\sigma_p^2}\left(\cos\left(\Omega t+\phi_p\right)+\cos\left(\Omega t+\phi_p-\Delta\phi\right)\right)}.\end{aligned} \tag{B.18}$$

Using (A.2), we get

$$s_x(t)=\sum_{i=1}^{8}A_i, \tag{B.19}$$

where

$$\begin{aligned}A_1&=\frac{\rho^2}{2\sigma_x^4}-\frac{\rho^2\gamma_x}{2\sigma_x^2}\cos(\Omega t+\phi_x)\\&\quad-\frac{\rho^2\gamma_x}{2\sigma_x^4}\cos(\Omega t+\phi_x-\Delta\phi),\end{aligned} \tag{B.20}$$

$$\begin{aligned}A_2&=\frac{\rho^2}{4\sigma_x^2}\cos(2\omega t)+\frac{\rho^2}{4\sigma_x^2}\cos(2\omega t-2\phi)\\&\quad-\frac{\rho^2}{2\sigma_x^2}\cos(\phi)\cos(2\omega t-\phi),\end{aligned} \tag{B.21}$$

$$\begin{aligned}A_3&=-\frac{\rho^2\gamma_x}{8\sigma_x^4}\cos((2\omega-\Omega)t-\phi_x)\\&\quad-\frac{\rho^2\gamma_x}{8\sigma_x^4}\cos((2\omega-\Omega)t-\phi_x+\Delta\phi),\end{aligned} \tag{B.22}$$

$$\begin{aligned}A_4&=-\frac{\rho^2\gamma_x}{8\sigma_x^2}\cos((2\omega-\Omega)t-2\phi-\phi_x+\Delta\phi)\\&\quad+\frac{\rho^2\gamma_x}{4\sigma_x^4}\cos((2\omega-\Omega)t-\phi-\phi_x),\end{aligned} \tag{B.23}$$

$$\begin{aligned}A_5&=\frac{\rho^2\gamma_x}{4\sigma_x^4}\cos(\phi)\cos((2\omega-\Omega)t-\phi-\phi_x+\Delta\phi)\\&\quad-\frac{\rho^2\gamma_x}{8\sigma_x^4}\cos((2\omega-\Omega)t-2\phi-\phi_x),\end{aligned} \tag{B.24}$$

$$\begin{aligned}A_6&=-\frac{\rho^2\gamma_x}{8\sigma_x^4}\cos((2\omega+\Omega)t+\phi_x)\\&\quad-\frac{\rho^2\gamma_x}{8\sigma_x^4}\cos((2\omega+\Omega)t+\phi_x-\Delta\phi),\end{aligned} \tag{B.25}$$

$$\begin{aligned}A_7&=-\frac{\rho^2\gamma_x}{8\sigma_x^4}\cos((2\omega+\Omega)t-2\phi+\phi_x)\\&\quad-\frac{\rho^2\gamma_x}{8\sigma_x^4}\cos((2\omega+\Omega)t-2\phi+\phi_x-\Delta\phi)\end{aligned} \tag{B.26}$$

and

$$\begin{aligned}A_8&=\frac{\rho^2\gamma_x}{4\sigma_x^4}\cos(\phi)\cos((2\omega+\Omega)t-\phi+\phi_x)\\&\quad+\frac{\rho^2\gamma_x}{4\sigma_x^4}\cos(\phi)\cos((2\omega+\Omega)t-\phi+\phi_x-\Delta\phi).\end{aligned} \tag{B.27}$$

The intermediate frequency is present in (B.22)–(B.24) and is equal to $\Delta\omega=2\omega-\Omega$.

Similarly, for $s_p(t)$,

$$s_p(t)=\sum_{i=1}^{8}A_i, \tag{B.28}$$

where

$$A_1 = \frac{\rho^2 m^2 \omega^2}{2\sigma_p^2}(1-\cos(\phi)) - \frac{\rho^2 m^2 \omega^2 \gamma_p}{2\sigma_p^4}\cos\left(\Omega t+\phi_p\right) - \frac{\rho^2 m^2 \omega^2 \gamma_p}{2\sigma_p^4}\cos\left(\Omega t+\phi_p-\Delta\phi\right), \quad \text{(B.29)}$$

$$A_2 = \frac{\rho^2 m^2 \omega^2 \gamma_p}{2\sigma_p^4}\cos(\phi)\cos\left(\Omega t+\phi_p\right) + \frac{\rho^2 m^2 \omega^2 \gamma_p}{2\sigma_p^4}\cos(\phi)\cos\left(\Omega t+\phi_p-\Delta\phi\right), \quad \text{(B.30)}$$

$$A_3 = -\frac{\rho^2 m^2 \omega^2}{2\sigma_p^2}\cos(2\omega t) - \frac{\rho^2 m^2 \omega^2}{2\sigma_p^2}\cos(2\omega t+2\phi) + \frac{\rho^2 m^2 \omega^2}{2\sigma_p^2}\cos(2\omega t+\phi), \quad \text{(B.31)}$$

$$A_4 = \frac{\rho^2 m^2 \omega^2 \gamma_p}{4\sigma_p^4}\cos\left((2\omega-\Omega)t-\phi_p\right) + \frac{\rho^2 m^2 \omega^2 \gamma_p}{4\sigma_p^4}\cos\left((2\omega-\Omega)t-\phi_p+\Delta\phi\right), \quad \text{(B.32)}$$

$$A_5 = \frac{\rho^2 m^2 \omega^2 \gamma_p}{4\sigma_p^4}\cos\left((2\omega-\Omega)t+2\phi-\phi_p\right) + \frac{\rho^2 m^2 \omega^2 \gamma_p}{4\sigma_p^4}\cos\left((2\omega-\Omega)t+2\phi-\phi_p+\Delta\phi\right), \quad \text{(B.33)}$$

$$A_6 = -\frac{\rho^2 m^2 \omega^2 \gamma_p}{4\sigma_p^4}\cos\left((2\omega-\Omega)t+\phi-\phi_p\right) - \frac{\rho^2 m^2 \omega^2 \gamma_p}{4\sigma_p^4}\cos\left((2\omega-\Omega)t+\phi-\phi_p+\Delta\phi\right), \quad \text{(B.34)}$$

$$A_7 = \frac{\rho^2 m^2 \omega^2 \gamma_p}{4\sigma_p^4}\cos\left((2\omega+\Omega)t+\phi_p\right) + \frac{\rho^2 m^2 \omega^2 \gamma_p}{4\sigma_p^4}\cos\left((2\omega+\Omega)t+\phi_p-\Delta\phi\right), \quad \text{(B.35)}$$

$$A_8 = \frac{\rho^2 m^2 \omega^2 \gamma_p}{4\sigma_p^4}\cos\left((2\omega+\Omega)t+2\phi+\phi_p\right) + \frac{\rho^2 m^2 \omega^2 \gamma_p}{4\sigma_p^4}\cos\left((2\omega+\Omega)t+2\phi+\phi_p-\Delta\phi\right) \quad \text{(B.36)}$$

and

$$A_9 = -\frac{\rho^2 m^2 \omega^2 \gamma_p}{4\sigma_p^4}\cos\left((2\omega+\Omega)t+\phi+\phi_p\right) - \frac{\rho^2 m^2 \omega^2 \gamma_p}{4\sigma_p^4}\cos\left((2\omega+\Omega)t+\phi+\phi_p-\Delta\phi\right). \quad \text{(B.37)}$$

The intermediate frequency $\Delta\omega = 2\omega - \Omega$ can be seen in (B.32)–(B.34).

References

[1] L. Rebuzzini, R. Artuso, S. Fishman, I. Guarneri, Effects of atomic interactions on quantum accelerator modes, Phys. Rev. A 76 (2007) 031603(R).
[2] C. Zhang, J. Liu, M.G. Raizen, Q. Niu, Transition to instability in a kicked Bose–Einstein condensate, Phys. Rev. Lett. 92 (2004) 054101.
[3] S. Moulieras, A.G. Monastra, M. Saraceno, P. Leboeuf, Wave-packet dynamics in nonlinear Schrödinger equations, Phys. Rev. A 85 (2012) 013841.
[4] M. Herrera, T.M. Antonsen, E. Ott, S. Fishman, Dynamic localization of a weakly interacting Bose–Einstein condensate in an anharmonic potential, Phys. Rev. A 87 (2013) 041603(R).
[5] A. Peres, Stability of quantum motion in chaotic and regular systems, Phys. Rev. A 30 (1984) 1610.
[6] R.A. Jalabert, H.M. Pastawski, Environmental-independent decoherence rate in classically chaotic systems, Phys. Rev. Lett. 86 (2001) 2490.
[7] P. Jacquod, I. Adagideli, C.W.J. Beenakker, Decay of the Loschmidt echo for quantum states with sub-Planck-scale structures, Phys. Rev. Lett. 89 (2002) 154103.
[8] N.R. Cerruti, S. Tomsovic, Sensitivity of wave field evolution and manifold stability in chaotic systems, Phys. Rev. Lett. 88 (2002) 054103.
[9] S. Wimberger, A. Buchleitner, Saturation of fidelity in the atom-optics kicked rotor, J. Phys. B 39 (2006) L145.
[10] M.F. Andersen, A. Kaplan, T. Grunzweig, N. Davidson, Decay of quantum correlations in atom optic billiards with chaotic and mixed dynamics, Phys. Rev. Lett. 97 (2006) 104102.
[11] A. Kaplan, M. Andersen, T. Grunzweig, N. Davidson, Hyperfine spectroscopy of optically trapped atoms, J. Opt. B 7 (2005) R103.
[12] M.F. Andersen, T. Grunzweig, A. Kaplan, N. Davidson, Revivals of coherence in chaotic atom-optics billiards, Phys. Rev. A 69 (2004) 063413.
[13] T. Gorin, T. Prosen, T.H. Seligman, M. Znidaric, Dynamics of Loschmidt echoes and fidelity decay, Phys. Rep. 435 (2006) 33.
[14] Y. Krivolapov, S. Fishman, E. Ott, T.M. Antonsen, Quantum chaos of a mixed open system of kicked cold atoms, Phys. Rev. E 83 (2011) 016204.
[15] M. Herrera, private communication, 2013.
[16] D.L. Shepelyansky, Delocalization of quantum chaos by weak nonlinearity, Phys. Rev. Lett. 70 (1993) 1787.
[17] M. Herrera, T.M. Antonsen, E. Ott, S. Fishman, Echoes and revival echoes in systems of anharmonically confined atoms, Phys. Rev. A 86 (2012) 023613.
[18] P. Milloni, M. Nieto, Coherent states, in: D. Greenberger, K. Hentschel, F. Weinert (Eds.), Compendium of Quantum Physics, Springer, Berlin, Heidelberg, 2009, pp. 106–108.